of abnormalities versus a unilateral abnormality. This drawback is compensated for by the *z*-score mapping with conventional GN using a low *z*-score threshold (e.g. 0 or 1).

Conclusion

In the present study, statistical *z*-score mapping with AI was more sensitive for detecting regional glucose hypometabolism and more accurate for identifying the side harboring the EZ using inter-ictal FDG-PET in unilateral MTLE than *z*-score mapping with conventional GN, when applied to the two approaches of peak analysis and extent analysis. Moreover, automated identification of the side harboring the EZ in unilateral MTLE was more accurate using a combination of statistical *z*-score mapping with AI and extent analysis based on VOIs of the parahippocampal gyrus.

References

1. Wiebe S, Blume WT, Girvin JP, Eliasziw M. A randomized, controlled trial of surgery for temporal-lobe epilepsy. N Engl J Med. 2001;345:311–88.
2. McIntosh AM, Kalnins RM, Mitchell LA, Fabinyi GC, Briellmann RS, Berkovic SF. Temporal lobectomy: long-term seizure outcome, late recurrence and risks for seizure recurrence. Brain. 2004;127:2018–30.
3. Lee DS, Lee JS, Kang KW, Jang MJ, Lee SK, Chung JK, et al. Disparity of perfusion and glucose metabolism of epileptogenic zones in temporal lobe epilepsy demonstrated by SPM/SPAM analysis on 15O water PET, [18F]FDG-PET, and [99mTc]-HMPAO SPECT. Epilepsia. 2001;42:1515–22.
4. Kim MA, Heo K, Choo MK, Cho JH, Park SC, Lee JD, et al. Relationship between bilateral temporal hypometabolism and EEG findings for mesial temporal lobe epilepsy: analysis of 18F-FDG PET using SPM. Seizure. 2006;15:56–63.
5. Kumar A, Juhasz C, Asano E, Sood S, Muzik O, Chugani HT. Objective detection of epileptic foci by 18F-FDG PET in children undergoing epilepsy surgery. J Nucl Med. 2010;51:1901–7.
6. Wong CH, Bleasel A, Wen L, Eberl S, Byth K, Fulham M, et al. The topography and significance of extratemporal hypometabolism in refractory mesial temporal lobe epilepsy examined by FDG-PET. Epilepsia. 2010;51:1365–73.
7. Ohta Y, Nariai T, Ishii K, Ishiwata K, Mishina M, Senda M, et al. Voxel- and ROI-based statistical analyses of PET parameters for guidance in the surgical treatment of intractable mesial temporal lobe epilepsy. Ann Nucl Med. 2008;22:495–503.
8. Kim YK, Lee DS, Lee SK, Kim SK, Chung CK, Chang KH, et al. Differential features of metabolic abnormalities between medial and lateral temporal lobe epilepsy: quantitative analysis of (18)F-FDG PET using SPM. J Nucl Med. 2003;44:1006–12.
9. Lee JJ, Kang WJ, Lee DS, Lee JS, Hwang H, Kim KJ, et al. Diagnostic performance of 18F-FDG PET and ictal 99mTc-HMPAO SPET in pediatric temporal lobe epilepsy: quantitative analysis by statistical parametric mapping, statistical probabilistic anatomical map, and subtraction ictal SPET. Seizure. 2005;14:213–20.
10. Van Bogaert P, Massager N, Tugendhaft P, Wikler D, Damhaut P, Levivier M, et al. Statistical parametric mapping of regional glucose metabolism in mesial temporal lobe epilepsy. Neuroimage. 2000;12:129–38.
11. Didelot A, Mauguiere F, Redoute J, Bouvard S, Lothe A, Reilhac A, et al. Voxel-based analysis of asymmetry index maps increases the specificity of 18F-MPPF PET abnormalities for localizing the epileptogenic zone in temporal lobe epilepsies. J Nucl Med. 2010;51:1732–9.
12. Engel J Jr, Van Ness PC, Rasmussen TB, Ojemann LM. Outcome with respect to epileptic seizure. In: Engel Jr J, editor. Surgical treatment of the epilepsies. 2nd ed. New York: Raven Press; 1993. p. 609–21.
13. Collins DL, Neelin P, Peters TM, Evans AC. Automatic 3D intersubject registration of MR volumetric data in standardized Talairach space. J Comput Assist Tomogr. 1994;18:192–205.
14. Talairach J, Tournoux P. Co-planar stereotaxic atlas of the human brain. New York: Thieme; 1988.
15. Sakai Y, Kumano H, Nishikawa M, Sakano Y, Kaiya H, Imabayashi E, et al. Cerebral glucose metabolism associated with a fear network in panic disorder. Neuroreport. 2005;16:927–31.
16. Fox PT, Mintun MA, Reiman EM, Raichle ME. Enhanced detection of focal brain responses using intersubject averaging and change-distribution analysis of subtracted PET images. J Cereb Blood Flow Metab. 1988;8:642–53.
17. Lancaster JL, Rainey LH, Summerlin JL, Freitas CS, Fox PT, Evans AC, et al. Automated labeling of the human brain: a preliminary report on the development and evaluation of a forward-transform method. Hum Brain Mapp. 1997;5:238–42.
18. Lancaster JL, Woldorff MG, Parsons LM, Liotti M, Freitas CS, Rainey L, et al. Automated Talairach Atlas labels for functional brain mapping. Hum Brain Mapp. 2000;10:120–31.
19. Brett M, Johnsrude IS, Owen AM. The problem of functional localization in the human brain. Nat Rev Neurosci. 2002;3:243–9.
20. Metz CE, Herman BA, Roe CA. Statistical comparison of two ROC-curve estimates obtained from partially-paired datasets. Med Decis Mak. 1998;18:110–21.
21. Kanetaka H, Matsuda H, Asada T, Ohnishi T, Yamashita F, Imabayashi E, et al. Effects of partial volume correction on discrimination between very early Alzheimer's dementia and controls using brain perfusion SPECT. Eur J Nucl Med Mol Imaging. 2004;31:975–80.
22. Minoshima S, Frey KA, Koeppe RA, Foster NL, Kuhl DE. A diagnostic approach in Alzheimer's disease using three-dimensional stereotactic surface projections of fluorine-18-FDG PET. J Nucl Med. 1995;36:1238–48.
23. Mizumura S, Kumita S, Cho K, Ishihara M, Nakajo H, Toba M, et al. Development of quantitative analysis method for stereotactic brain image: assessment of reduced accumulation in extent and severity using anatomical segmentation. Ann Nucl Med. 2003;17:289–95.
24. Matsuda H, Mizumura S, Nagao T, Ota T, Iizuka T, Nemoto K, et al. Automated discrimination between very early Alzheimer disease and controls using an easy Z-score imaging system for multicenter brain perfusion single-photon emission tomography. Am J Neuroradiol. 2007;28:731–6.
25. Yanase D, Matsunari I, Yajima K, Chen W, Fujikawa A, Nishimura S, et al. Brain FDG PET study of normal aging in Japanese: effect of atrophy correction. Eur J Nucl Med Mol Imaging. 2005;32:794–805.
26. Kawachi T, Ishii K, Sakamoto S, Matsui M, Mori T, Sasaki M. Gender differences in cerebral glucose metabolism: a PET study. J Neurol Sci. 2002;199:79–83.

Neurol Sci (2012) 33:1355–1364
DOI 10.1007/s10072-012-0949-5

ORIGINAL ARTICLE

State-dependent precursors of seizures in correlation-based functional networks of electrocorticograms of patients with temporal lobe epilepsy

Hirokazu Takahashi · Shuhei Takahashi · Ryohei Kanzaki · Kensuke Kawai

Received: 1 October 2011 / Accepted: 10 January 2012 / Published online: 21 January 2012

Abstract Accurate prediction of epileptic seizures will open novel therapeutic possibilities for patients with intractable epilepsy. We attempted to identify precursors of seizures in the functional networks of electrocorticograms by applying graph theory. Long-term electrocorticograms for periods of 39–76 h from three patients with temporal lobe epilepsy were investigated using pair-wise cross-correlations. Time-varying network properties suggested that there were several distinct brain states. Although functional networks during seizures could be characterized as having a regular topography, no consistent characteristics of functional networks were found immediately prior to seizure onsets. However, it was found that seizures under an identical state were followed by similar transients of the network properties. These results suggest that network properties themselves could not serve as reliable predictors of seizure onset. Yet, some significant pre-seizure changes in the parameters tested appear likely to depend on the brain state. To predict seizures, it may be necessary to take into consideration the states of the brain. In addition to stationary network properties we characterized in the present study, dynamic interactions of epileptic activities with the network might be taken into account to predict the spread of a seizure.

Keywords Graph theory · Electrocorticogram · Epilepsy · Seizure prediction · Seizure detection

H. Takahashi · R. Kanzaki
Research Center for Advanced Science and Technology, The University of Tokyo, Komaba 4-6-1, Meguro-ku, Tokyo 153-8904, Japan

H. Takahashi · S. Takahashi · R. Kanzaki
Graduate School of Information Science and Technology, The University of Tokyo, Hongo 7-3-1, Bunkyo-ku, Tokyo 113-8656, Japan

H. Takahashi
PRESTO, JST, 4-1-8 Honcho Kawaguchi, Saitama 332-0012, Japan

K. Kawai (✉)
Department of Neurosurgery, Graduate School of Medicine, The University of Tokyo, Hongo 7-3-1, Bunkyo-ku, Tokyo 113-8655, Japan
e-mail: kenkawai-tky@umin.net

Introduction

Accurate prediction of epileptic seizures will bring considerable benefits for a significant population of patients with drug-resistant and intractable epilepsy. For example, warnings of oncoming seizure would reduce the grave threats posed by sudden, unforeseen seizures. Furthermore, on-demand interventions such as direct electrical stimulation or biofeedback could be established as novel therapeutic options to prevent seizures [1–4].

Seizure prediction based on scalp electroencephalogram (EEG) results has long been attempted since the 1970s [5], in which correlations to systematic preictal changes in linear [6–8] and non-linear parameters [9–11] have been explored. Despite these extensive efforts, prediction accuracy has thus far never been sufficiently reliable for practical use.

Recently, an increasing number of studies have investigated prediction based on intra-cranial EEG, or electrocorticogram (ECoG) results, which provide a significantly better signal-to-noise ratio and spatial resolution than scalp EEGs. Some of these studies suggest that potential seizure precursors are widely distributed in areas remote from the

Table 1 Subjects

	Age at surgery	Gender	Location of epileptic focus	Type of seizure	Outcome of surgery (Engel class)	# of seizure during recording	Total recording time (hours)
Pt #1	40	M	Left mediobasal temporal lobe	SP, CP, SG	Id	2	39
Pt #2	47	M	Right lateral temporal lobe	SP, CP, SG	Ia	2	67
Pt #3	36	F	Left temporal tip/uncus	SP, CP	Ia	5	76

SP simple partial, *CP* complex partial, *SG* secondarily generalized

Table 2 Locations of implanted electrodes

Subject	Electrode #	Hemisphere	Location
Pt #1	#1–#4	Left (*LH*)	Uncus (*un*)
	#5–#12		Mediobasal temporal lobe (*mb*)
	#13–#16		Posterobasal temporal lobe (*pb*)
	#17–#22		Orbitofrontal surface (*os*)
	#23–#70		Lateral temporal lobe (*lt*)
	#71–#78	Right (*RH*)	Mediobasal temporal lobe
	#79–#86		Lateral temporal lobe
Pt #2	#1–#4	Left	Uncus
	#5–#12		Mediobasal temporal lobe
	#13–#16		Posterobasal temporal lobe
	#17–#22		Broca's area (*Br*)
	#23–#70		Lateral temporal lobe
	#71–#74	Right	Uncus
	#75–#82		Mediobasal temporal lobe
	#83–#86		Posterobasal temporal lobe
	#87–#92		Broca's area
	#93–#120		Lateral temporal lobe
Pt #3	#1–#4	Left	Temporal tip (*tt*)
	#5–#8		Uncus
	#9–#16		Mediobasal temporal lobe
	#17–#24		Posterobasal temporal lobe
	#25–#30		Hippocampus (*hc*)
	#31–#74		Lateral temporal lobe
	#75–#82		Uncus
	#75–#82	Right	Mediobasal temporal lobe
	#83–#90		Lateral temporal lobe

Abbreviations as used in Fig. 4

epileptic focus, occasionally in the contralateral hemisphere [12–16]. This suggests an emphasis be placed on functional network properties that allow seizures to spread. Therefore, multi-variate measures such as inter-electrode correlation and synchrony have come to be considered better predictors of seizure onset than conventional univariate measures [17–19]. These multi-variate measures can be summarized as global network properties using a graph theory approach. The global network properties can potentially serve as useful predictors [20, 21].

Furthermore, recent growth in storage capacity for data has made viable continuous multi-day recordings, which provide an opportunity to investigate confounding variables such as circadian fluctuation of bodily state and vigilance state [22–24]. These variables have long been considered to affect the ability to predict seizures [7], but have not yet been intensively investigated.

In the current study, with a goal of improving seizure prediction, we investigate long-term ECoG results of patients suffering from temporal lobe epilepsy. First of all, we characterize how the state of the brain varies hour by hour in terms of global properties of correlation-based functional networks. Secondly, we attempt to identify precursors of seizures in these functional networks. Thirdly, we test whether these precursors depend on the brain state.

Materials and methods

Subjects

Three patients (Patient #1–Patient #3) were randomly selected from a group that underwent surgical treatment for drug-resistant epilepsy (Table 1). The patients selected had seizures that involved the medial or lateral temporal lobe at onset and that had comparable seizure patterns. All patients had a comprehensive presurgical evaluation including a detailed history review and neurological examination, neuropsychological testing, scalp EEG with sphenoidal leads, magnetoencephalography, magnetic resonance imaging (MRI), fluoro-2-deoxy-D-glucose positron emission tomography, Technetium-99m ethyl cysteinate dimer single photon emission computed tomography (SPECT) (123)I-iomazenil SPECT, and long-term ECoG monitoring with multiple subdural electrodes. Abolishment of seizures was verified based on postsurgical observation for two or more years in all patients.

Long-term ECoG recordings

Electrocorticogram recording was performed during long-term video-ECoG monitoring in the University of Tokyo Hospital. It was carried out as a part of the patient's routine clinical care. Informed consent was obtained from all patients for implantation of intracranial electrodes, surgical treatment, and separately for research use of the ECoG data. Research use of ECoG data, including this study, was approved by the local ethical committee.

Following temporal craniotomy, grid electrodes were placed on the lateral frontotemporal cortices. For the mediobasal temporal region, a trapezoid grid with eight contacts aligned in a T-shape fashion was used in combination with strip electrodes. Using fluoroscopy to align the four medial contacts of the trapezoid grid at the same height as and just behind the tip of the dorsum sellae enabled the four contacts to cover the parahippocampal gyrus in the anteroposterior direction. Table 2 shows the locations of the implanted electrodes. Figure 1 shows the representative overlaying images of 3D reconstruction from the computed tomography (CT) and MRI of Patient #1.

The original reference electrode is a scalp reference Cz. Signals were simultaneously monitored at all of the active electrodes by a 128-channel EEG recording system (Nicolet) without any digital filtering and stored on a hard disk with an A/D resolution of 16 bits/sample and a sample rate of 400 Hertz (Hz).

The EEG signals were first visually analyzed by an experienced epileptologist/epilepsy surgeon (K.K), and typical seizures were selected. Video images of the patients around the time of the EEG seizures were inspected as well. Only seizures in which an EEG seizure preceded or started simultaneously with clinical signs of a seizure were included in this study.

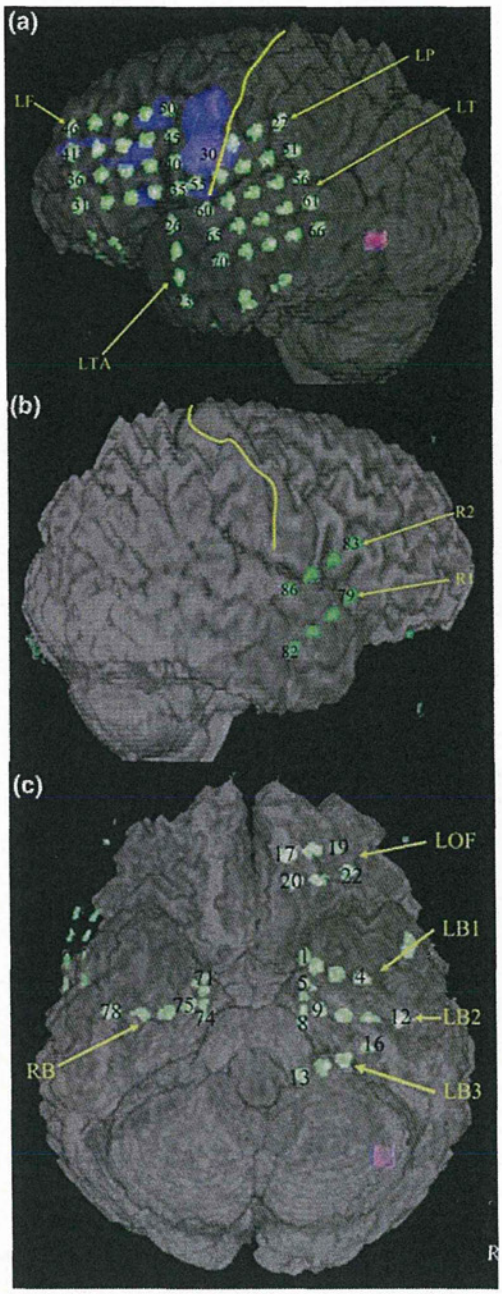

Fig. 1 Representative 3D reconstruction from computed tomography (CT) overlaying CT and MRI images of patient (Pt.) #1. **a** Left side. **b** Right side. **c** Base

Data analysis

For specific frequency bands, functional networks within n recording sites, or n nodes (n = 86–120), were estimated

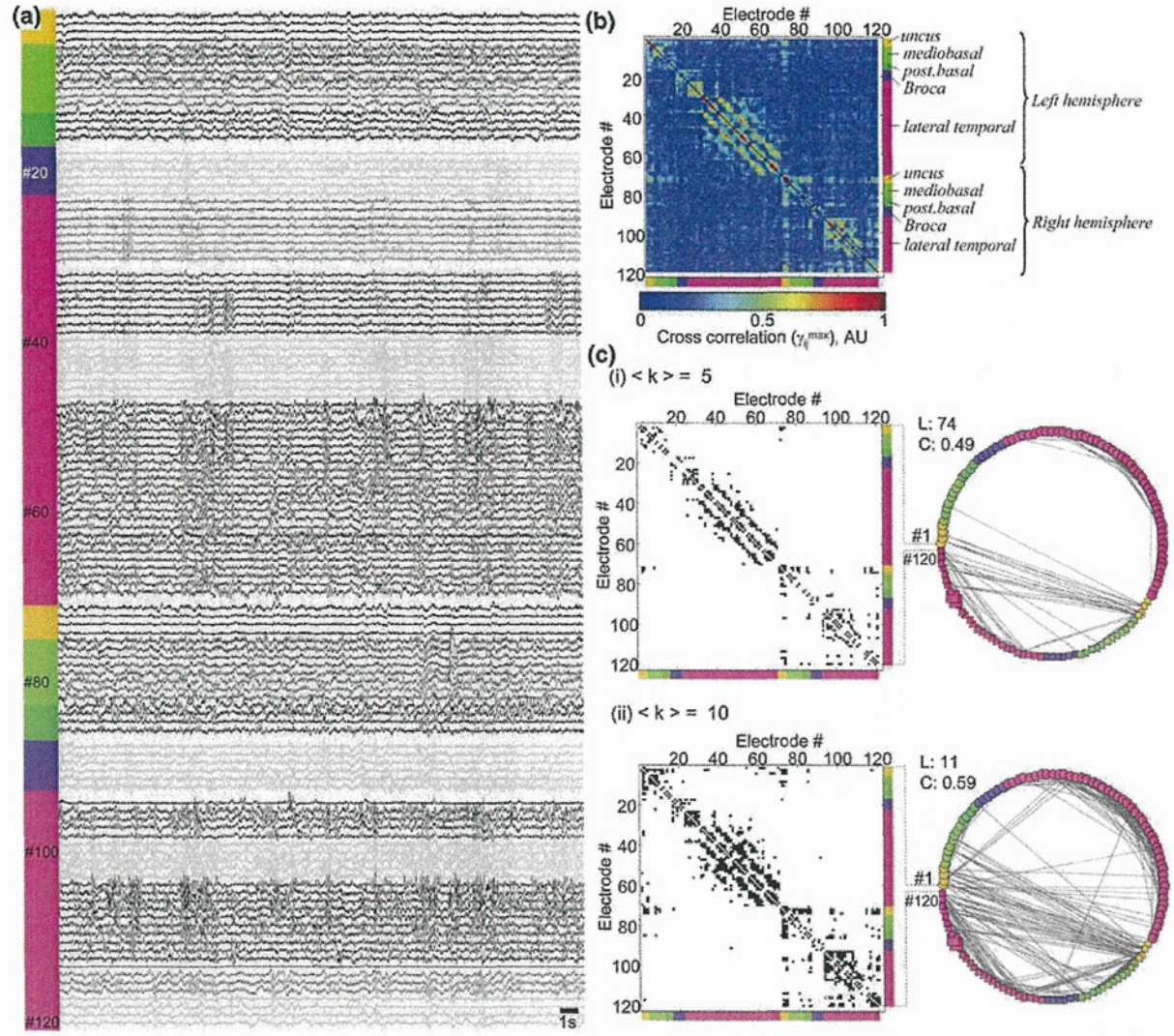

Fig. 2 Analytical procedure. **a** ECoG signals in a representative sliding window. The signals were aligned according to the identification number of the electrode (#1–#120). Regions of each electrode are designated by a *ticked band* at the *left* edge as defined in (**b**). Signals from an identical electrode array within a given area are drawn in the same gray level. **b** Matrix of normalized cross-correlation function, $\gamma_{ij}^{\max}$. The location of each electrode is indicated in the *right* margin. **c** Adjacency matrices, a_{ij} (*left*), and graph structures of functional networks (*right*). The threshold, T, to binarize $\gamma_{ij}^{\max}$ was determined according to the average degree of graph: **i** $\langle k \rangle = 5$; and **ii** $\langle k \rangle = 10$. A filled element in the adjacency matrices indicates that a link exists between the corresponding nodes. Markers in the graphs correspond to recording sites (#1–#120), and the *ticked markers* indicate regions as defined in (**b**). *Circles* and *squares* in the graphs indicate nodes in the left and right hemispheres of the brain, respectively, and large markers indicate the locations of epileptic foci. On the upper *left* hand of the graph, the values of L and C are indicated

on the basis of a pair-wise measurement of maximum linear cross-correlation and characterized on the basis of graph theory [20, 21].

Electrocorticogram signals were first divided into five frequency bands by FFT filters: δ 1–3 Hz; θ 4–7 Hz; α 8–13 Hz; β 14–30 Hz; and γ 30–64 Hz. In each band, functional links between any pair of recording sites $(i, j \in [1, n])$ were defined in a given sliding window using the following normalized cross-correlation function:

$$\gamma_{ij}^{\max} = \max_{\tau} \left\{ \frac{c(x_i, x_j)(\tau)}{\sqrt{c(x_i, x_i)(0)\, c(x_j, x_j)(0)}} \right\}$$

where

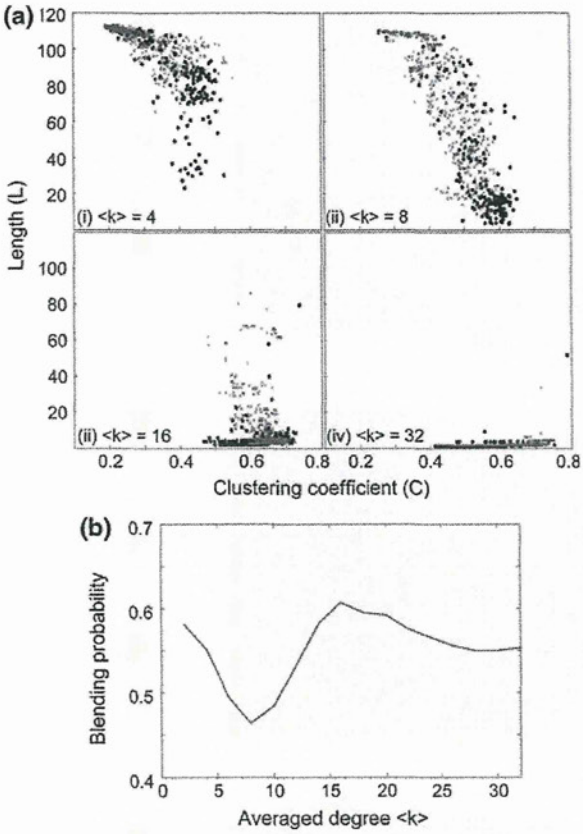

Fig. 3 Optimization of average degree. **a** Distribution of the average shortest path length, L, and the average cluster coefficient, C, at various values of $\langle k \rangle$. *Dark circles* and *light crosses* correspond to samples from pre-seizure states and interictal states, respectively. **b** Blending probability of pre-seizure state compared with interictal state as a function of $\langle k \rangle$

Table 3 $\langle k \rangle$ used as threshold in network characterization

	Delta	Theta	Alpha	Beta	Gamma
Pt #1	6	6	6	10	8
Pt #2	12	10	8	8	6
Pt #3	14	10	6	8	10

$$c(x_i, x_j)(\tau) = \begin{cases} \sum_{t=1}^{w-\tau} x_i(t+\tau)\, x_j(t), & \tau \geq 0 \\ c(x_j, x_i)(-\tau), & \tau < 0 \end{cases}$$

denotes the linear cross-correlation function quantifying the similarity of two signals x_i and x_j with a time lag of τ. $\gamma_{ij}^{\max}$ is confined to [0, 1] with high values indicating the two signals have a similar course over time though there is a possible time lag. The duration of the sliding window, w, was relatively long, 25 s in the current study, in order to characterize temporally stable links. The duration of the step of sliding was in increments of 60 s for the entire long-term data sets, and 1 s for data for the time period within 20 min before or after the clinical onset of seizures.

$\gamma_{ij}^{\max}$ was then binarized according to an arbitrary threshold, T, and the adjacency matrix, a_{ij}, was derived:

$$a_{ij} = \begin{cases} 1, & i \neq j \wedge \gamma_{ij}^{\max} \geq T \\ 0 & \text{otherwise.} \end{cases}$$

Based on a_{ij}, the properties of this functional network, or graph, were characterized in terms of degree distribution, average shortest path length, and cluster coefficient. The degree at each node was defined as:

$$k_i = \sum_{j=1}^{n} a_{ij}.$$

The average shortest path length was defined as:

$$L = \frac{2}{n(n-1)} \sum_{i>j} d_{ij}$$

where d_{ij} is the smallest number of links that can connect nodes i and j. When there was no path between two nodes, $d_{ij} = n$ was adopted. As a measure of the typical separation between two nodes in the graph, L is thus confined to $[1, n]$.

The cluster coefficient at node i was defined as:

$$C_i = \frac{2}{k_i(k_i-1)} E_i$$

where k_i denotes the number of nodes with a direct link from node i, and thus k_i $(k_i-1)/2$ means the number of allowable links within these k_i neighboring nodes, and E_i denotes the total number of links that actually exist in the neighboring nodes. The cluster coefficient of the network was then determined as.

$$C = \frac{1}{n} \sum_{i=1}^{n} E_i$$

C is confined to [0, 1], evaluating the cliquishness of a typical neighborhood.

Because L and C depended on T, T was optimized such that distributions of L and C in pre-seizure periods became most distinct from those in interictal periods. Sample distributions in L–C plane were first estimated for the pre-seizure group and interictal group. The pre-seizure group included samples from 10-min period before the first onset of clinical seizures with a time step of 1 s, and the interictal group was sampled from the whole dataset with a time step of 20 min. This distribution of L and C from either pre-seizure group or interictal group was used to estimate a probability of the corresponding group membership for each sample, assuming that the squared Mahalanobis' generalized distance in L–C plane is distributed as Chi-squared with 2 degree of freedom. For all of pre-seizure samples, the probability of interictal group membership

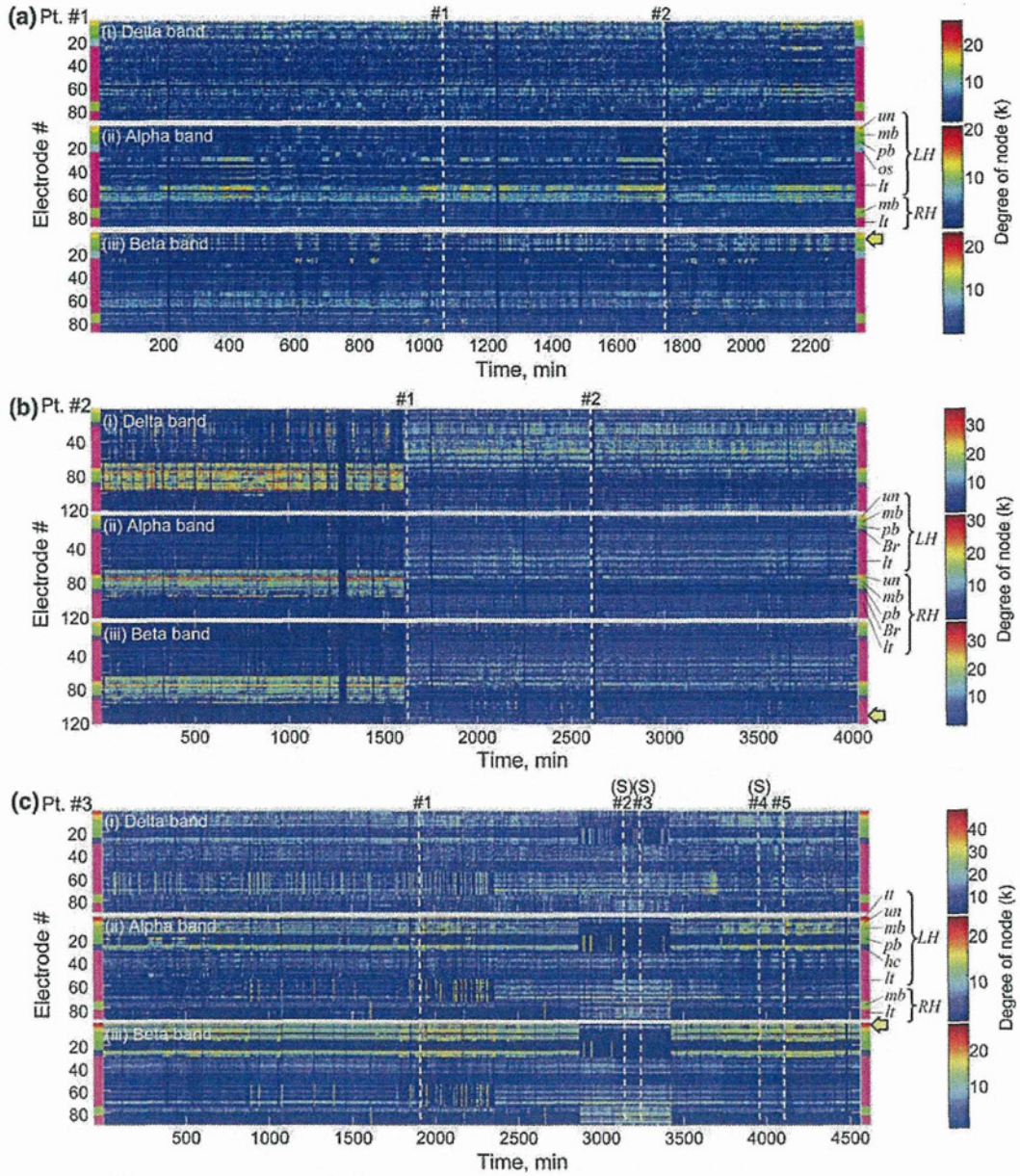

Fig. 4 Long-term characterization of degree distribution for each subject: **a** Pt. #1, **b** Pt. #2, **c** Pt. #3. The degree distributions shown are obtained at the indicated time and electrode for the indicated frequency bands: **i** delta, **ii** alpha, **iii** beta. Abbreviated locations of each electrode are indicated on the *right* and are defined in Table 2. A *broken line* indicates the occurrence of a seizure. Some seizures were simple partial seizures (labeled S), while others were complex partial seizures

was averaged to evaluate how often samples from the pre-seizure period belonged to interictal periods, and this average probability was defined as a blending probability. The blending probability was obtained as a function of the average degree. Because a low blending probability suggests that the properties of graphs, i.e., L and C, during the pre-seizure period are distinct from those during interictal periods, T was determined such that the graph has the optimal average degree, where the lowest blending probability was achieved.

Results

Figure 2a shows ECoG signals in a representative sliding window, from which the alpha-band cross-correlation

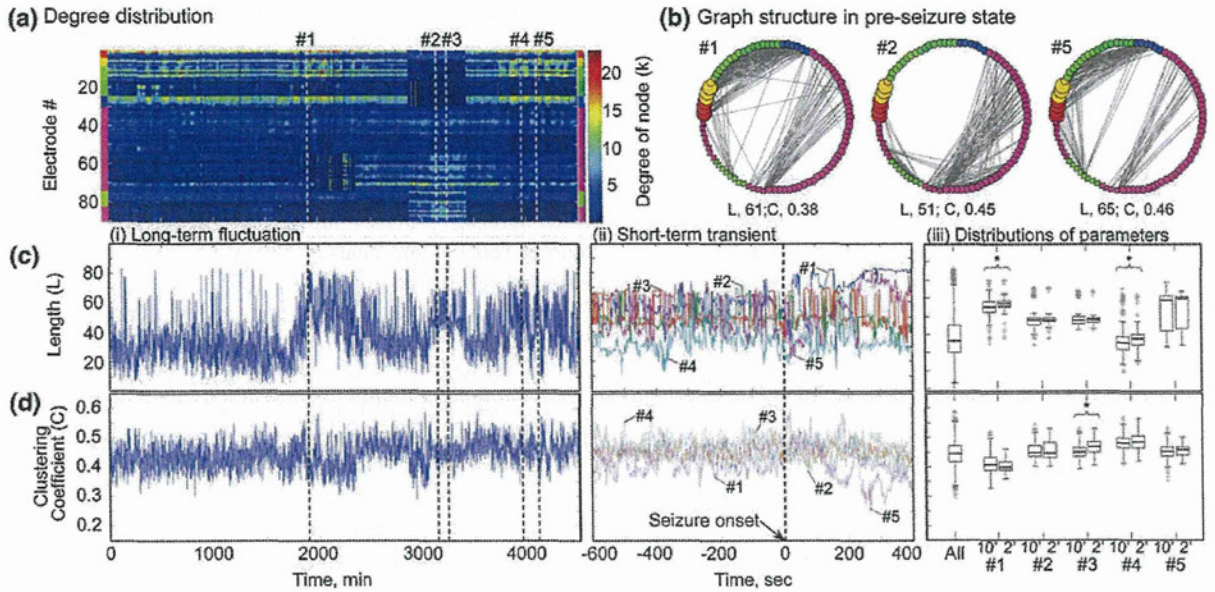

Fig. 5 Representative analyses in the alpha band for Pt. #3. **a** Degree distribution. **b** Graph structures at 10 min prior to onset of seizures #1, #2 and #3. The values of L and C are indicated at the *bottom* of each graph. **c** Average shortest path length (L): **i** Long-term characterization, **ii** Short-term transient characterization around the time of the onset of seizures, **iii** Distribution for the entire period, and for pre-seizure periods of two minutes (2′) and ten minutes (10′) before the onset of each seizure (#1–#5). On each *box*, the central mark is the median, and the edges of the *box* are the 25 and 75th percentiles. The whiskers extend to the most extreme data points not considered outliers. Data points that are larger than the 75th percentile or smaller than the 25th percentile by 1.5 times the inter-quartile range were considered to be outliers. The outliers were plotted individually using a '+' mark. An *asterisk* indicates statistical significance between a given pair (Mann–Whitney's U test; $^*p < 0.01$). **d** Average cluster coefficient (C)

matrix, $\gamma_{ij}^{\max}$, was obtained as shown in Fig. 2b. Most of the high correlations were found around the diagonal, indicating that nearby sites in the same anatomically defined region tended to be tightly linked, yet some pairs between inter-areal or inter-hemispherical sites also showed relatively high correlations. In order to characterize the properties of $\gamma_{ij}^{\max}$ as a graph, two representative adjacent matrices, a_{ij}, were obtained in Figs. 2c i, ii, in which the thresholds were determined such that the average degrees of nodes $\langle k_i \rangle$ became five and ten, respectively, demonstrating how a_{ij}, and thereby, the properties (L and C), as well as the structure of graphs, depended on the threshold.

At different thresholds, Fig. 3a shows how L and C were distributed over a long time scale during interictal periods and also in a confined pre-seizure period of 10 min before the first onset of clinical seizures. From these plots, the blending probabilities were derived as a function of average degree as shown in Fig. 3b. The optimal average degree was then determined, where the blending probability was minimized. Table 3 shows thus-obtained average degrees, which are used below to characterize a functional network in each frequency band for each patient.

For each patient Fig. 4 shows how a degree of node was distributed among recording sites in the band-specific functional networks and how the distributions of degree changed with time. For example, in patient #1, high-degree recording sites were often found in the alpha band within a confined region in the left lateral temporal lobe, thus potentially serving as a hub in this network (Fig. 4a, ii), while epileptic foci in the left mediobasal temporal lobe had relatively high degrees in the delta and beta bands (Fig. 4a, i, iii). In addition, in patients #2 and #3, the patterns of degree distribution, k_i, suggest that there are several distinct brain states. In patient #2, high-degree recording sites moved from the right hemisphere to the left hemisphere during the recording (Fig. 4b). Both of the seizures in patient #2 occurred in the latter state with high-degree sites in the left hemisphere. In patient #3, the brain states were likely to vary from hour to hour, and seizures did not always occur under a specific state; i.e., degree distribution patterns for seizures #1, #4 and #5 appeared to be distinct from those for seizures #2 and #3 (Fig. 4c). These states are long-lasting on the order of a day (e.g., in Pt. #2, >2400 min after seizure #1; in Pt. #3, >2700 min from the beginning of recording) and thus may not be attributed to shorter changes of state such as sleep cycle, wake/sleep cycle, or vigilance states.

In Fig. 5, representative analyses in the alpha band of patient #3 show how the structure and properties of functional networks depend on the states defined by the degree

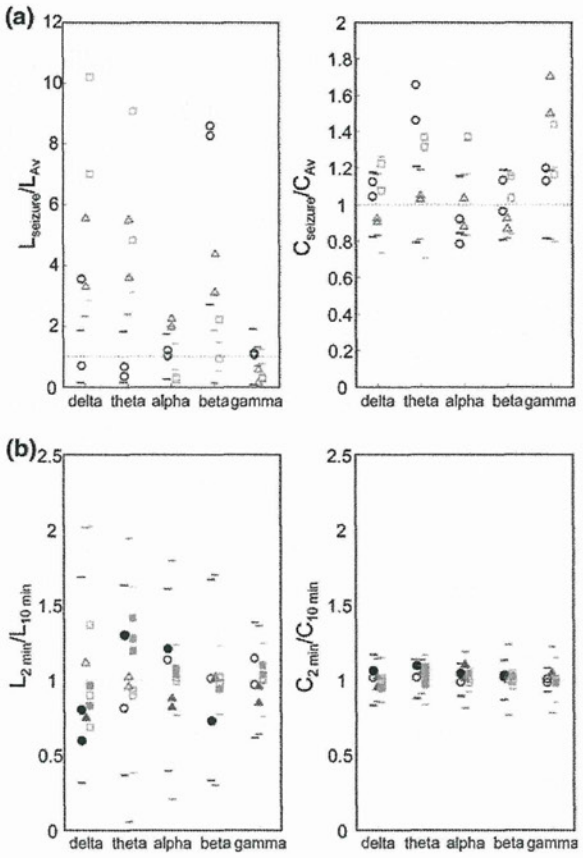

Fig. 6 Band-specific characterization of L and C. **a** Values of L and C during complex partial seizures ($L_{seizure}$ and $C_{seizure}$) were compared to those averaged over the long-term (L_{Av} and C_{Av}). Standard deviations of $L_{seizure}/L_{Av}$ and $C_{seizure}/C_{Av}$ are indicated by *small lines* for each patient in each band. **b** Values of L and C 2 min before seizures (L_{2min} and C_{2min}) were compared to those 10 min (L_{10min} and C_{10min}) before seizures. Symbols indicate subjects as follows: *circle* Pt. #1, *triangle* Pt. #2, *square* Pt. #3. *Filled symbols* indicate significant changes (see Table 4)

distribution in Fig. 5a. As shown in Fig. 5b, the structure of the functional network at 10 min prior to seizure #2 was distinct from those prior to seizures #1 and #5, confirming a close link between network structure and brain state. Figure 5c, i; d, i show the variation of L and C with time over a long timeframe. The results suggest that global trends may be associated with a change of brain states. The transient traces of L and C around the time of the onset of each seizure are plotted in Fig. 5c, ii; d, ii, respectively, in order to examine whether these properties serve as a predictor of seizures. From these data, boxplots in Fig. 5c, iii; d, iii show the distributions of L and C, respectively, for the timeframes indicated. In some parameters, distribution 10 min (10′) and 2 min (2′) before seizure onset were significantly different (Mann–Whitney's U test, $p < 0.01$). Specifically, increases in L were seen just before impending seizures #1 and #4 and increases in C preceded seizure #3. These parameters may be predictive signs of seizures.

In Fig. 6a, L and C during complex partial seizures ($L_{seizure}$ and $C_{seizure}$) were compared to L and C averaged over the long term (L_{Av} and C_{Av}). Aberrant values during seizures were often observed to be large L and C values, corroborating previous reports that functional networks during seizures are characterized as having a consistent, rather than random, topology [20, 21].

Similarly, in Fig. 6b, the averages of L and C 2 min before the onset of seizures (i.e., L_{2min} and C_{2min}) were compared with those 10 min before the onset of seizures (i.e., L_{10min} and C_{10min}). In comparison to apparent alterations of network properties during seizures (Fig. 6a), the differences in L and C 10 min and 2 min before the onset of seizures were less clear, yet there were significant differences in some parameters when L_{2min} and C_{2min} were compared to L_{10min} and C_{10min}, respectively (Mann–Whitney's U test, $p < 0.01$). For all seizures observed, Table 4 summarizes band-specific significant changes of L_{2min} and C_{2min} compared to L_{10min} and C_{10min}, respectively. These results indicate that in some cases L and C decrease rather than increase prior to the onset of seizures, suggesting that, unlike during seizures, pre-seizure states cannot be characterized as a shift toward regular networks. The directions of significant changes in L and C were sometimes different among seizures within an identical subject, yet were likely identical under similar states as defined by degree distribution (Fig. 4). Verification of this hypothesis entails testing 60 possible pairs of parameters since there are ten parameters (i.e., L and C each for 5 frequency bands) and 6 possible pairs of seizures with the same state (i.e., 1 for patient. #1, 1 for patient #2, and 4 for patient #3 [seizure sets #1 and #4, #1 and #5, #4 and #5, and #2 and #3]). Among these 60 possible pairs with the same state, nine pairs showed identical changes (5 *L*s and 4 *C*s) while only one pair showed an opposite change (C in delta band of patient #2), suggesting that, within identical states, consistent changes of the network parameters immediately preceding the onset of a seizure, if any, are not a coincidence (i.e., 9/60 vs. 1/60; z test, $p = 0.00104$).

Discussion

In the current study, we have characterized long-term ECoG signals on the basis of pair-wise cross-correlations, and attempted to identify precursors of seizures in terms of functional network properties (Fig. 2). First, time-varying network properties suggested that there were several distinct brain states. Because these states lasted for more than

Table 4 Significant pre-seizure changes of band-specific L and C found in each patient

	Pt #1				Pt #2			
	L		C		L		C	
	#1	#2	#1	#2	#1	#2	#1	#2
Delta	▼	▼		△	▼		△	▼
Theta	△			△	▼	▼	△	△
Alpha	△		△				△	△
Beta		▼	△					
Gamma					▼	▼		△

	Pt #3									
	L					C				
	#1	#2	#3	#4	#5	#1	#2	#3	#4	#5
Delta		▼	▼				▼			
Theta			△	△	△	▼	△	△	▼	
Alpha	△			△				△		
Beta		▼					△			△
Gamma			△		△					▼

△ increase, ▼ decrease (Mann–Whitney's U test, $p < 0.01$)

a day (e.g., in Pt. #2, >2400 min after seizure #1; in Pt. #3, >2700 min from the beginning of recording), they were likely unrelated to sleep cycle, wake/sleep cycle or vigilance state (Fig. 4). Second, while functional networks during seizure were possible to characterize as having a consistent topography, no consistent characteristics of functional networks were found immediately prior to the onset of seizures, indicating that network properties themselves could not serve as reliable precursors for predicting the onset of seizures (Figs. 5, 6). Yet, our data suggest that significant pre-seizure changes, if any, depended on the brain state: that is, seizures under an identical brain state were likely to be followed by similar transient network properties (Table 4).

The duration of the sliding window, w, and the threshold, T, that were used to transform $\gamma_{ij}^{\max}$ into a_{ij} are ad hoc parameters in the current study. The selected length of w is a tradeoff between stationarity of analyses and temporal resolution. A long window size of 25 s was adopted in our analyses to extract reliable functional networks; shortening w, on the other hand, might enhance sensitivity to precursors prior to seizures. The structure of functional networks also substantially depends on T (Fig. 2c). A large T extracts reliable functional networks, but in turn results in a sparse graph, for which network properties cannot be properly characterized. For example, to estimate small-world properties, $\langle k_i \rangle$ should be larger than $\ln(n)$ [e.g., for $n = 120$ (patient #2), $\langle k_i \rangle$ should be greater than 4.79] [25]. On the other hand, if T is small, the functional networks are likely to contain unimportant, distracting links. The blending probability was thus introduced in the present analyses as a practical, well-balanced solution to objectively determine the T at which the network properties in the pre-seizure period become most distinct from those in an interictal state (Fig. 3). The adequacy of the range of thus-derived values for T (i.e., 6–14) confirmed the appropriateness of this method. Furthermore, large L and C during seizure were consistent with existing reports [20, 21], verifying that our analysis is able to adequately extract state-dependent network properties.

The current study demonstrated only limited effectiveness in terms of seizure prediction, but helps give direction for future studies. First, the study suggests that consideration of brain states may be required for seizure prediction. Limited success to date despite extensive attempts to predict seizures may be partly the result of overlooking the possibility that many precursors are state-dependent. Mormann et al. [14, 15] found relatively consistent seizure precursors with anticipation time on the order of 1 h. Therefore, identification of the presentiment state of seizure may be a vital step in seizure prediction. Second, global properties such as k_i, L and C can be used for characterizing states, but not for predicting transient shifts from pre-seizure states to ictal states. Previous studies also reported poor predictive abilities of global properties via either graph theory [20, 21] or other multi-variate measures [18]. Instead, local synchrony between specific electrode pairs may be more useful for prediction [14, 15, 19, 26]. Furthermore, dynamic interactions of epileptic activities [27–30] with pre-determined functional networks should be

taken into account in attempts to predict the extent of seizure spreading [17, 31].

Acknowledgment This work was financially supported partly by the Ministry of Health, Labour and Welfare of Japan (Grant for Comprehensive Research on Disability, Health and Welfare; H23-Nervous and Muscular-General-003).

Conflict of interest The authors do not have any conflict of interest to be declared.

References

1. Elger CE (2001) Future trends in epileptology. Curr Opin Neurol 14(2):185–186
2. Theodore WH, Fisher RS (2004) Brain stimulation for epilepsy. Lancet Neurol 3(2):111–118
3. Osorio I, Frei MG, Sunderam S, Giftakis J, Bhavaraju NC, Schaffner SF, Wilkinson SB (2005) Automated seizure abatement in humans using electrical stimulation. Ann Neurol 57(2):258–268
4. Morrell M (2006) Brain stimulation for epilepsy: can scheduled or responsive neurostimulation stop seizures? Curr Opin Neurol 19(2):164–168
5. Mormann F, Andrzejak RG, Elger CE, Lehnertz K (2007) Seizure prediction: the long and winding road. Brain 130(Pt 2):314–333
6. Rogowski Z, Gath I, Bental E (1981) On the prediction of epileptic seizures. Biol Cybern 42(1):9–15
7. Siegel A, Grady CL, Mirsky AF (1982) Prediction of spike-wave bursts in absence epilepsy by EEG power-spectrum signals. Epilepsia 23(1):47–60
8. Salant Y, Gath I, Henriksen O (1998) Prediction of epileptic seizures from two-channel EEG. Med Biol Eng Comput 36(5):549–556
9. Iasemidis LD, Sackellares JC, Zaveri HP, Williams WJ (1990) Phase space topography and the Lyapunov exponent of electrocorticograms in partial seizures. Brain Topogr 2(3):187–201
10. Martinerie J, Adam C, Le Van Quyen M, Baulac M, Clemenceau S, Renault B, Varela FJ et al (1998) Epileptic seizures can be anticipated by non-linear analysis. Nat Med 4(10):1173–1176
11. Le Van Quyen M, Martinerie J, Navarro V, Boon P, D'Have M, Adam C, Renault B, Varela F, Baulac M (2001) Anticipation of epileptic seizures from standard EEG recordings. Lancet 357(9251):183–188
12. D'Alessandro M, Esteller R, Vachtsevanos G, Hinson A, Echauz J, Litt B (2003) Epileptic seizure prediction using hybrid feature selection over multiple intracranial EEG electrode contacts: a report of four patients. IEEE Trans Biomed Eng 50(5):603–615
13. D'Alessandro M, Vachtsevanos G, Esteller R, Echauz J, Cranstoun S, Worrell G, Parish L, Litt B (2005) A multi-feature and multi-channel univariate selection process for seizure prediction. Clin Neurophysiol 116(3):506–516
14. Mormann F, Kreuz T, Andrzejak RG, David P, Lehnertz K, Elger CE (2003) Epileptic seizures are preceded by a decrease in synchronization. Epilepsy Res 53(3):173–185
15. Mormann F, Kreuz T, Rieke C, Andrzejak RG, Kraskov A, David P, Elger CE, Lehnertz K (2005) On the predictability of epileptic seizures. Clin Neurophysiol 116(3):569–587
16. Esteller R, Echauz J, D'Alessandro M, Worrell G, Cranstoun S, Vachtsevanos G, Litt B (2005) Continuous energy variation during the seizure cycle: towards an on-line accumulated energy. Clin Neurophysiol 116(3):517–526
17. Wendling F, Bartolomei F, Bellanger JJ, Bourien J, Chauvel P (2003) Epileptic fast intracerebral EEG activity: evidence for spatial decorrelation at seizure onset. Brain 126(Pt 6):1449–1459
18. Schindler K, Leung H, Elger CE, Lehnertz K (2007) Assessing seizure dynamics by analysing the correlation structure of multichannel intracranial EEG. Brain 130(Pt 1):65–77
19. Kuhlmann L, Freestone D, Lai A, Burkitt AN, Fuller K, Grayden DB, Seiderer L, Vogrin S, Mareels IM, Cook MJ (2010) Patient-specific bivariate-synchrony-based seizure prediction for short prediction horizons. Epilepsy Res 91(2–3):214–231
20. Ponten SC, Bartolomei F, Stam CJ (2007) Small-world networks and epilepsy: graph theoretical analysis of intracerebrally recorded mesial temporal lobe seizures. Clin Neurophysiol 118(4):918–927
21. Schindler KA, Bialonski S, Horstmann MT, Elger CE, Lehnertz K (2008) Evolving functional network properties and synchronizability during human epileptic seizures. Chaos 18(3):033119
22. Lehnertz K (1999) Non-linear time series analysis of intracranial EEG recordings in patients with epilepsy—an overview. Int J Psychophysiol 34(1):45–52
23. Kreuz T, Andrzejak RG, Mormann F, Kraskov A, Stogbauer H, Elger CE, Lehnertz K, Grassberger P (2004) Measure profile surrogates: a method to validate the performance of epileptic seizure prediction algorithms. Phys Rev E Stat Nonlin Soft Matter Phys 69(6 Pt 1):061915
24. Navarro V, Martinerie J, Le Van Quyen M, Baulac M, Dubeau F, Gotman J et al (2005) Seizure anticipation: do mathematical measures correlate with video-EEG evaluation? Epilepsia 46(3):385–396
25. Watts DJ, Strogatz SH (1998) Collective dynamics of 'small-world' networks. Nature 393(6684):440–442
26. Winterhalder M, Schelter B, Maiwald T, Brandt A, Schad A, Schulze-Bonhage A, Timmer J (2006) Spatio-temporal patient-individual assessment of synchronization changes for epileptic seizure prediction. Clin Neurophysiol 117(11):2399–2413
27. Bragin A, Engel J Jr, Wilson CL, Fried I, Mathern GW (1999) Hippocampal and entorhinal cortex high-frequency oscillations (100–500 Hz) in human epileptic brain and in kainic acid-treated rats with chronic seizures. Epilepsia 40(2):127–137
28. Huberfeld G, Menendez de la Prida L, Pallud J, Cohen I, Le Van Quyen M, Adam C, Clemenceau S, Baulac M, Miles R et al (2011) Glutamatergic pre-ictal discharges emerge at the transition to seizure in human epilepsy. Nat Neurosci 14(5):627–634
29. Truccolo W, Donoghue JA, Hochberg LR, Eskandar EN, Madsen JR, Anderson WS, Brown EN, Halgren E, Cash SS (2011) Single-neuron dynamics in human focal epilepsy. Nat Neurosci 14(5):635–641
30. Yaari Y, Beck H (2002) "Epileptic neurons" in temporal lobe epilepsy. Brain Pathol 12(2):234–239
31. Lago-Fernandez LF, Huerta R, Corbacho F, Siguenza JA et al (2000) Fast response and temporal coherent oscillations in small-world networks. Phys Rev Lett 84(12):2758–2761

See the corresponding editorial in this issue, pp 1219–1220.

J Neurosurg 116:1221–1225, 2012

Delayed complication after Gamma Knife surgery for mesial temporal lobe epilepsy

Clinical article

KENICHI USAMI, M.D.,[1] KENSUKE KAWAI, M.D., PH.D.,[1] TOMOYUKI KOGA, M.D., PH.D.,[1] MASAHIRO SHIN, M.D., PH.D.,[1] HIROKI KURITA, M.D., PH.D.,[2] ICHIRO SUZUKI, M.D., PH.D.,[3] AND NOBUHITO SAITO, M.D., PH.D.[1]

[1]Department of Neurosurgery, The University of Tokyo Hospital, Tokyo; [2]Department of Cerebrovascular Surgery, Saitama Medical University International Medical Center, Saitama; and [3]Department of Neurosurgery, Japanese Red Cross Medical Center, Tokyo, Japan

Object. Despite the controversy over the clinical significance of Gamma Knife surgery (GKS) for refractory mesial temporal lobe epilepsy (MTLE), the modality has attracted attention because it is less invasive than resection. The authors report long-term outcomes for 7 patients, focusing in particular on the long-term complications.

Methods. Between 1996 and 1999, 7 patients with MTLE underwent GKS. The 50% marginal dose covering the medial temporal structures was 18 Gy in 2 patients and 25 Gy in the remaining 5 patients.

Results. High-dose treatment abolished the seizures in 2 patients and significantly reduced them in 2 others. One patient in this group was lost to follow-up. However, 2 patients presented with symptomatic radiation necrosis (SRN) necessitating resection after 5 and 10 years. One patient who did not need necrotomy continued to show radiation necrosis on MRI after 10 years. One patient died of drowning while swimming in the sea 1 year after GKS, before seizures had disappeared completely.

Conclusions. High-dose treatment resulted in sufficient seizure control but carried a significant risk of SRN after several years. Excessive target volume was considered as a reason for delayed necrosis. Drawbacks such as a delay in seizure control and the risk of SRN should be considered when the clinical significance of this treatment is evaluated. *(http://thejns.org/doi/abs/10.3171/2012.2.JNS111296)*

KEY WORDS • Gamma Knife surgery • mesial temporal lobe epilepsy • delayed complication • symptomatic radiation necrosis • oncology

ACCUMULATING evidence suggests that surgical treatment for intractable MTLE achieves favorable outcomes,[6,20,23] and medial temporal lobectomy is generally the first choice for the treatment of intractable MTLE. However, as a complete elimination of the complications associated with craniotomy is difficult, GKS has attracted attention as an alternative to craniotomy. Gamma Knife surgery for AVMs,[10] glioma,[5,18,19] and other intracranial lesions associated with epilepsy has shown antiepileptic effects, which have since been applied in cases of intractable MTLE. Gamma Knife surgery for MTLE was first performed by Régis et al.,[16] and it began to be used at several other facilities in the late 1990s.[2,4,11,15,17,21] Recently, a multicenter randomized study with a 3-year follow-up demonstrated that GKS offered seizure remission rates comparable to those of open surgery,[1] while a second report with 8 years of follow-up failed to demonstrate that GKS successfully controls seizures over the long term.[22] The clinical significance of GKS for MTLE remains undetermined, and its role in the treatment of MTLE needs to be further evaluated for efficacy and safety.

In this article, we report the long-term outcomes of 7 patients who underwent GKS for MTLE, and we consider the potential for the development of delayed complications.

Abbreviations used in this paper: AVM = arteriovenous malformation; CPS = complex partial seizure; GKS = Gamma Knife surgery; MTLE = mesial temporal lobe epilepsy; SRN = symptomatic radiation necrosis.

Methods

Patient Population

Our protocol for GKS in patients with intractable epilepsy was approved by the ethics committee of the University of Tokyo in August 1996.[11] Between December

1996 and August 1999, 7 patients were diagnosed with intractable MTLE; 6 patients had hippocampal sclerosis, and 1 patient had cavernous hemangioma. All patients underwent presurgical evaluations that included CT scanning, MRI, ictal and interictal SPECT, FDG-PET, and simultaneous video-electroencephalography recording. The side of epileptogenic focus could not be determined in 3 of the 7 patients after these noninvasive examinations, including a patient with interictal spikes from the contralateral side of the lesion on MRI and 2 patients with bilateral hippocampal accumulation in ictal SPECT. Thus, these patients underwent the placement of bilateral intracranial electrodes, and the side of epileptic focus was confirmed (Table 1).

Gamma Knife Surgery Protocol

The 50% isodose line covered the amygdala, hippocampal head and body, most of the parahippocampal gyrus, and the entorhinal cortex (Fig. 1). The marginal dose at 50% isodose was 18 Gy in the first 2 cases (low-dose group). Eight isocenters with an 8-mm collimator and 3 isocenters with a 14-mm collimator were used in the patient in Case 1, and 8 isocenters with an 8-mm collimator and 4 isocenters with a 14-mm collimator were used in the patient in Case 2. Because the low-dose protocol was not effective in these 2 patients, the marginal dose was increased to 25 Gy, and 4 isocenters with an 18-mm collimator were used in the remaining 5 patients (high-dose group). We used the radiosurgical planning software KULA (Elekta Instruments) until September 1998 (in Cases 1–4); thereafter, GammaPlan (Elekta Instruments) was used (in Cases 5–7).

Follow-Up

After GKS, all patients were observed for seizure frequency and complications, and postoperative changes were evaluated by periodic MRI examinations.

Results

Low-Dose Group

The patients in the low-dose GKS group (Cases 1 and 2) had no seizure reduction by 30 months (Case 1) and 16 months (Case 2). Both patients underwent an anterior medial temporal lobectomy. Each patient experienced complete seizure remission immediately after surgery. Detailed descriptions of the early low-dose group have been reported elsewhere.[11]

High-Dose Group

In the high-dose group (Cases 3–7), CPSs had disappeared in 2 patients (Cases 3 and 4) and were significantly decreased in 2 patients (Cases 5 and 7); however, the patient in Case 7 died of drowning while swimming in the sea 1 year after GKS. One patient was lost to follow-up (Case 6). Two patients who became CPS free required a craniotomy due to SRN after long-term recovery following GKS.

The patient in Case 3 developed mild headache 6 months after GKS. A small area of edema and slight contrast enhancement in the temporal lobe were noted on MRI 10 months after GKS. The patient was subsequently prescribed steroids to treat the persistent headache and for the enlargement of the enhanced lesion with diffuse edema on MRI. After steroid administration, the enhanced lesion and edema did not expand, but it also did not disappear. After 5 years, the patient developed generalized convulsive seizures, and MRI showed that necrosis and diffuse edema remained (Fig. 2). The patient underwent a necrotomy, which abolished her seizures completely. The resected specimen showed radiation necrosis without malignant tumor cells.

The patient in Case 4 presented with gait disturbance 8 years after GKS, and MRI revealed hydrocephalus, augmentation of necrosis, and extension of edema. At this time she underwent ventriculoperitoneal shunt placement, which improved her hydrocephalus. However, necrosis and edema continued to expand, and a necrotomy was performed 2 years after ventriculoperitoneal shunt placement (Fig. 3). She became seizure free after surgery. The resected specimen revealed radiation necrosis without malignant tumor cells.

The patient in Case 5 has not reported about symptoms caused by an increase in intracranial pressure associated with SRN after GKS. However, the lesion, which enhanced on Gd administration, cyst formation, and perifocal edema were still noted on the MRI studies 10 years after GKS (Fig. 4). At present, the patient has a few seizure attacks a year.

TABLE 1: Patient characteristics*

Case No.	Age (yrs), Sex	FC	Intracranial Electrode	Age at Seizure Onset (yrs)	MRI Atrophy	Hypometabolism	Seizure Origin on Video-EEG	GKS Side
1	31, F	yes	yes	6	rt	no laterality	rt	rt
2	22, M	yes	no	9	rt	rt	rt	rt
3	30, F	yes	yes	22	lt	bilat	lt	lt
4	66, F	no	no	45	rt	rt	rt	rt
5	33, F	yes	yes	18	rt	rt	rt	rt
6	24, F	no	no	15	rt	rt	rt	rt
7	41, M	yes	no	12	rt	rt	rt	rt

* EEG = electroencephalography; FC = febrile convulsion.

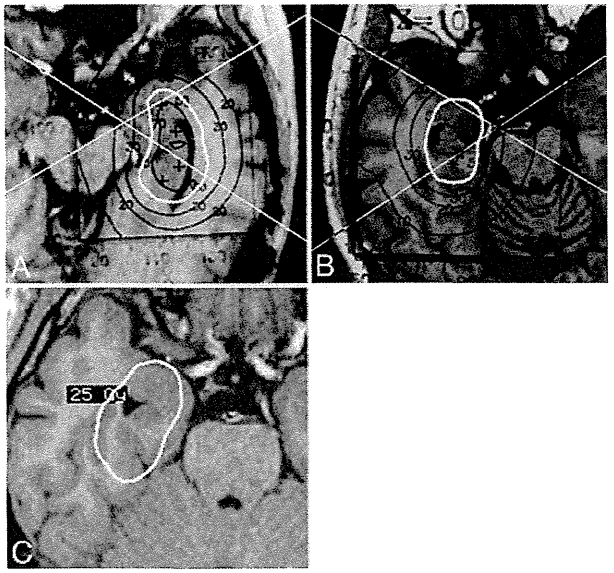

FIG. 1. Dose planning for Cases 3 (A), 4 (B), and 5 (C). The 50% isodose line *(white line)* covers the amygdala, hippocampal head, body, parahippocampal gyrus, and entorhinal cortex.

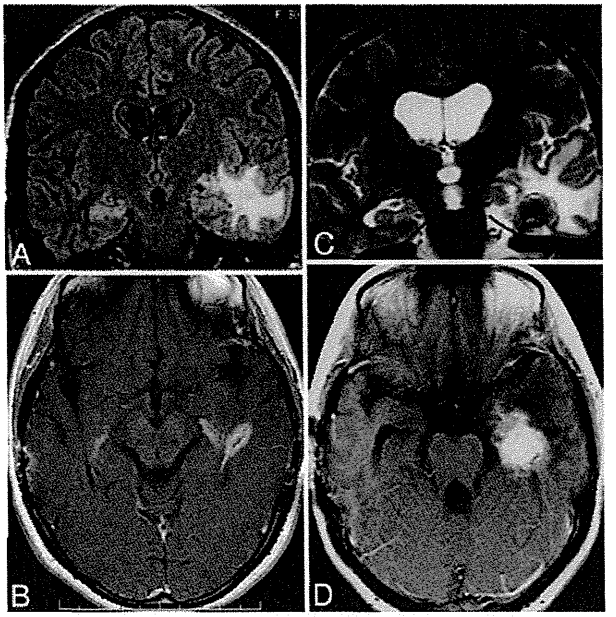

FIG. 2. Case 3. Magnetic resonance images. Coronal FLAIR (A) and axial Gd-enhanced (B) images obtained 10 months after GKS showing small areas of edema in the temporal lobe and a Gd-enhanced lesion in the medial temporal lobe. Coronal T2-weighted (C) and axial Gd-enhanced (D) images obtained 5 years after GKS showing augmentation of necrosis in the medial temporal lobe and diffuse edema around the area of necrosis.

Discussion

We observed SRN in 2 of 5 patients who underwent high-dose GKS for MTLE. Although the CPSs in 2 patients with SRN were controlled, the patients required a necrotomy 5 and 10 years after GKS because of SRN. In most cases of GKS for MTLE, a lesion and surrounding edema transiently were reported to appear approximately 1 year after GKS and gradually regressed within a few years.[3,15] New headaches were noted in 70% of cases, but most of them could be controlled by steroids.[1] Although Barbaro et al.[1] concluded that GKS was a safe alternative to craniotomy in a patient population evaluated over a 3-year follow-up period, 1 patient who received 24 Gy underwent medial temporal lobectomy early after GKS for worsening papillary edema despite steroid administration. Although Bartolomei et al.[2] reported the longest series of GKS for MTLE, no SRN was noted. While there was a 1-Gy difference between their protocol and ours, we emphasize the importance of long-term follow-up in this treatment, since we experienced delayed SRN presenting more than 5 years after GKS.

Predictive factors for radiation necrosis after GKS have been studied in cases of AVM and tumor.[7,12] According to Kjellberg et al.[12] and Flickinger et al.,[7] the predictive factors for radiation necrosis were associated with dose and volume. The 50% isodose volume ranged from 5500 to 9000 mm^3 in a previously reported protocol for MTLE,[1,2,15,17] whereas in our cases, isodose volumes in Cases 3, 4, and 5 were 12,000, 7800, and 8300 mm^3, respectively. The target area of previous reports included the anterior part of the medial temporal lobe, whereas in our cases these areas extended posteriorly, which provided such a difference in the target volume. The volume in the patient in Case 3 was much higher than that in previously reported protocols, and even the volumes in the patients in Cases 4 and 5 were slightly higher (Table 2). One possible reason why SRN occurred in a delayed phase might be the increased irradiation volume. Too large a target volume might make the radiation necrosis remain over a long period.

Delayed SRN was observed after GKS for AVM.[8,14,24] However, predictive factors for the delayed occurrence of radiation necrosis have not been determined. Meanwhile, in thalamotomy, in which the target is the brain parenchyma as in MTLE, the radiation dose is considerably higher, ranging from 100 to 200 Gy, but the irradiated volume is too low to result in SRN.[9,13]

Whereas craniotomy for MTLE can achieve control of seizures immediately after surgery, there is a delay in antiseizure effects after GKS; in previous studies, an average of 10–12 months was reported to have elapsed until seizure control.[1,2,15] The patient in Case 7, whose seizures were decreasing, died of drowning 1 year after GKS. Srikijvilaikul et al.[21] reported that 2 of 5 patients died of unexplained causes before seizure control after GKS. The delay of seizure control is a critical drawback of GKS for patients with epilepsy.

We judged that GKS had no curative effect at 30 and 16 months after GKS in the earlier 2 cases in the low-dose protocol, and craniotomy was performed in these patients. In the series of Vojtech et al.,[22] 7 of 14 patients underwent medial temporal lobectomy after GKS due to a lack of efficacy. The average waiting period was 63.5 months. The time course for seizure reduction or cessation is another undetermined issue.

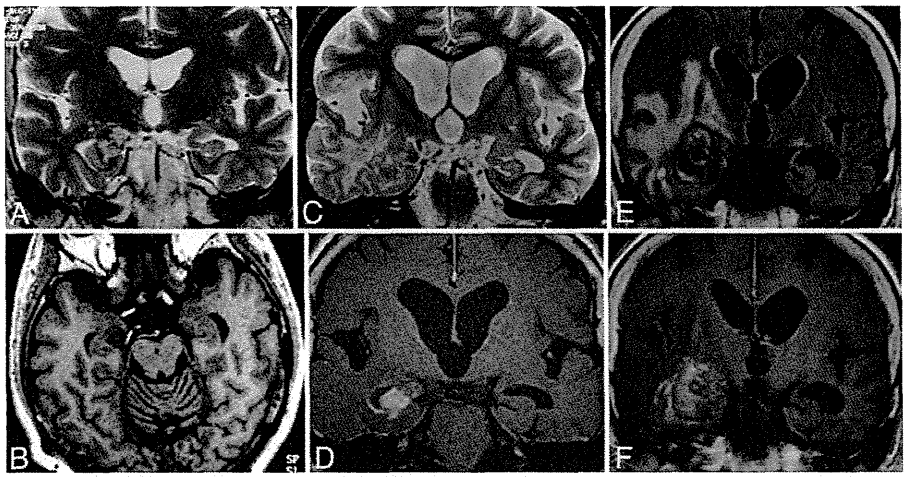

Fig. 3. Case 4. Magnetic resonance images. Coronal T2-weighted **(A)** and axial T1-weighted **(B)** images obtained before GKS showing a cavernous malformation in the right mesial temporal lobe. Coronal T2-weighted **(C)** and Gd-enhanced **(D)** images obtained 8 years after GKS showing hydrocephalus, a small area of radiation necrosis, and edema in the temporal lobe. Coronal FLAIR **(E)** and Gd-enhanced **(F)** images obtained 10 years after GKS showing improvement in hydrocephalus but deterioration of radiation necrosis and edema.

Conclusions

Two of our patients had SRN that required craniotomy more than 5 years after GKS for MTLE. Excessive target volume was presumed as the possible reason of SRN. One patient died suddenly before achieving seizure control. Medial temporal lobectomy results in favorable outcomes for intractable MTLE. Currently, the indications for consideration of GKS as an alternative to surgery are limited to a few cases that may be inoperable. When performing GKS, careful consideration of the proper target area is needed. Delayed SRN and seizure remission should be kept in mind, and it is necessary to continue to monitor patients' progress carefully and for a long time. Further studies with controlled protocols are needed to determine whether GKS should be offered for patients with MTLE.

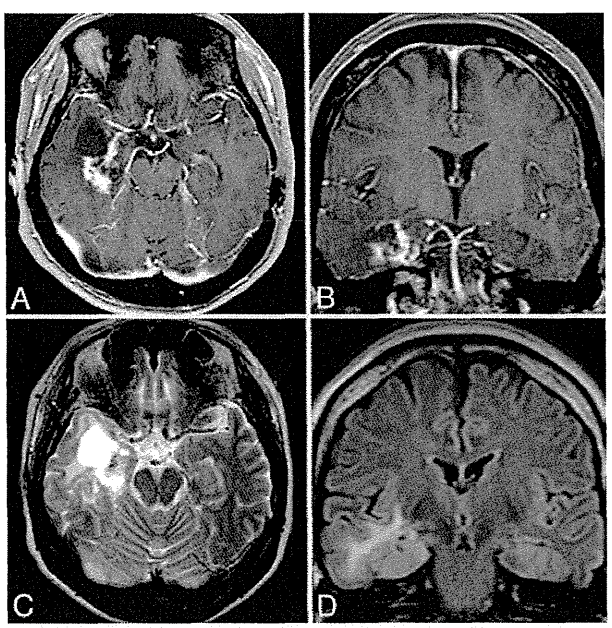

Fig. 4. Case 5. Magnetic resonance images. Gadolinium-enhanced **(A and B)**, T2-weighted **(C)**, and FLAIR **(D)** images obtained 10 years after GKS show that a Gd-enhanced lesion and surrounding edema in the temporal lobe remain and cyst formation is observed in the temporal lobe.

Disclosure

The authors report no conflict of interest concerning the materials or methods used in this study or the findings specified in this paper.

Author contributions to the study and manuscript preparation include the following. Conception and design: Kawai, Suzuki. Acquisition of data: Usami, Koga, Shin, Kurita, Suzuki, Saito. Analysis and interpretation of data: Usami, Kawai. Drafting the article: Usami. Critically revising the article: all authors. Reviewed submitted version of manuscript: all authors. Approved the final version of

TABLE 2: Summary of the literature regarding irradiation dose and 50% isodose volume

Authors & Year	No. of Cases	50% Isodose (Gy)	50% Isodose Vol (mm^3)
Régis et al., 1999	7	25	6,250–6,900
Bartolomei et al., 2008	15	24 ± 1	5,500–9,000
Rheims et al., 2008	15	21.1 ± 2.6	6,960 ± 1,250
Barbaro et al., 2009	30	20 or 24	5,500–7,500
present series			
Case 3		25	12,000
Case 4		25	7,800
Case 5		25	8,300
Case 6		25	8,900
Case 7		25	12,300

the manuscript on behalf of all authors: Usami. Study supervision: Kawai, Suzuki, Saito.

References

1. Barbaro NM, Quigg M, Broshek DK, Ward MM, Lamborn KR, Laxer KD, et al: A multicenter, prospective pilot study of gamma knife radiosurgery for mesial temporal lobe epilepsy: seizure response, adverse events, and verbal memory. **Ann Neurol 65:**167–175, 2009
2. Bartolomei F, Hayashi M, Tamura M, Rey M, Fischer C, Chauvel P, et al: Long-term efficacy of gamma knife radiosurgery in mesial temporal lobe epilepsy. **Neurology 70:**1658–1663, 2008
3. Chang EF, Quigg M, Oh MC, Dillon WP, Ward MM, Laxer KD, et al: Predictors of efficacy after stereotactic radiosurgery for medial temporal lobe epilepsy. **Neurology 74:**165–172, 2010
4. Cmelak AJ, Abou-Khalil B, Konrad PE, Duggan D, Maciunas RJ: Low-dose stereotactic radiosurgery is inadequate for medically intractable mesial temporal lobe epilepsy: a case report. **Seizure 10:**442–446, 2001
5. De Riu PL, Rocca A: Interstitial irradiation therapy of supratentorial gliomas by stereotaxic technique. Long term results. **Ital J Neurol Sci 9:**243–248, 1988
6. Engel J Jr, Wiebe S, French J, Sperling M, Williamson P, Spencer D, et al: Practice parameter: temporal lobe and localized neocortical resections for epilepsy: report of the Quality Standards Subcommittee of the American Academy of Neurology, in association with the American Epilepsy Society and the American Association of Neurological Surgeons. **Neurology 60:**538–547, 2003
7. Flickinger JC, Schell MC, Larson DA: Estimation of complications for linear accelerator radiosurgery with the integrated logistic formula. **Int J Radiat Oncol Biol Phys 19:**143–148, 1990
8. Foroughi M, Kemeny AA, Lehecka M, Wons J, Kajdi L, Hatfield R, et al: Operative intervention for delayed symptomatic radionecrotic masses developing following stereotactic radiosurgery for cerebral arteriovenous malformations—case analysis and literature review. **Acta Neurochir (Wien) 152:**803–815, 2010
9. Friehs GM, Park MC, Goldman MA, Zerris VA, Norén G, Sampath P: Stereotactic radiosurgery for functional disorders. **Neurosurg Focus 23(6):**E3, 2007
10. Heikkinen ER, Konnov B, Melnikov L, Yalynych N, Zubkov YN, Garmashov YA, et al: Relief of epilepsy by radiosurgery of cerebral arteriovenous malformations. **Stereotact Funct Neurosurg 53:**157–166, 1989
11. Kawai K, Suzuki I, Kurita H, Shin M, Arai N, Kirino T: Failure of low-dose radiosurgery to control temporal lobe epilepsy. **J Neurosurg 95:**883–887, 2001
12. Kjellberg RN, Hanamura T, Davis KR, Lyons SL, Adams RD: Bragg-peak proton-beam therapy for arteriovenous malformations of the brain. **N Engl J Med 309:**269–274, 1983
13. Okun MS, Stover NP, Subramanian T, Gearing M, Wainer BH, Holder CA, et al: Complications of gamma knife surgery for Parkinson disease. **Arch Neurol 58:**1995–2002, 2001
14. Oyoshi T, Hirahara K, Uetsuhara K, Yatsushiro K, Arita K: Delayed radiation necrosis 7 years after gamma knife surgery for arteriovenous malformation—two case reports. **Neurol Med Chir (Tokyo) 50:**62–66, 2010
15. Régis J, Bartolomei F, Rey M, Genton P, Dravet C, Semah F, et al: Gamma knife surgery for mesial temporal lobe epilepsy. **Epilepsia 40:**1551–1556, 1999
16. Régis J, Peragui JC, Rey M, Samson Y, Levrier O, Porcheron D, et al: First selective amygdalohippocampal radiosurgery for 'mesial temporal lobe epilepsy.' **Stereotact Funct Neurosurg 64 (Suppl 1):**193–201, 1995
17. Rheims S, Fischer C, Ryvlin P, Isnard J, Guenot M, Tamura M, et al: Long-term outcome of gamma-knife surgery in temporal lobe epilepsy. **Epilepsy Res 80:**23–29, 2008
18. Rogers LR, Morris HH, Lupica K: Effect of cranial irradiation on seizure frequency in adults with low-grade astrocytoma and medically intractable epilepsy. **Neurology 43:**1599–1601, 1993
19. Rossi GF, Scerrati M, Roselli R: Epileptogenic cerebral low-grade tumors: effect of interstitial stereotactic irradiation on seizures. **Appl Neurophysiol 48:**127–132, 1985
20. Spencer SS, Berg AT, Vickrey BG, Sperling MR, Bazil CW, Shinnar S, et al: Predicting long-term seizure outcome after resective epilepsy surgery: the multicenter study. **Neurology 65:**912–918, 2005
21. Srikijvilaikul T, Najm I, Foldvary-Schaefer N, Lineweaver T, Suh JH, Bingaman WE: Failure of gamma knife radiosurgery for mesial temporal lobe epilepsy: report of five cases. **Neurosurgery 54:**1395–1404, 2004
22. Vojtech Z, Vladyka V, Kalina M, Nespor E, Seltenreichová K, Semnická J, et al: The use of radiosurgery for the treatment of mesial temporal lobe epilepsy and long-term results. **Epilepsia 50:**2061–2071, 2009
23. Wiebe S, Blume WT, Girvin JP, Eliasziw M: A randomized, controlled trial of surgery for temporal-lobe epilepsy. **N Engl J Med 345:**311–318, 2001
24. Yamamoto M, Hara M, Ide M, Ono Y, Jimbo M, Saito I: Radiation-related adverse effects observed on neuro-imaging several years after radiosurgery for cerebral arteriovenous malformations. **Surg Neurol 49:**385–398, 1998

Manuscript submitted August 4, 2011.
Accepted February 14, 2012.
Please include this information when citing this paper: published online March 23, 2012; DOI: 10.3171/2012.2.JNS111296.
Address correspondence to: Kenichi Usami, M.D., Department of Neurosurgery, Faculty of Medicine, The University of Tokyo, 7-3-1 Hongo, Bunkyo-ku, Tokyo 113-8655, Japan. email: usaken-tky@umin.ac.jp.

BRAIN and NERVE 64(9) : 1013-1022, 2012

特 集 ■ 高次脳機能イメージングの脳科学への新展開

てんかん外科治療における高次脳機能イメージングの役割

Role of Functional Neuroimaging in the Surgical Treatment of Epilepsy

川 合 謙 介*

Kensuke Kawai*

Abstract

Functional neuroimaging is one of the most progressing fields in neuroscience and clinical neurological practice. It has also been contributing to the diagnosis and treatment of epilepsy. Intracranial electroencephalography (iEEG) is the gold standard for the diagnostic localization of the epileptogenic zone in the surgical treatment of epilepsy. Currently, no other modalities, including novel functional neuroimaging modalities, are superior to iEEG in sensitivity and spatial resolution. However, iEEG is an invasive procedure and its clinical usefulness is dependent on appropriate coverage of the epileptogenic zone. In this review article, the author discusses the principles of decision making in surgical indication and procedures by presenting clinical cases and evaluating the significance of functional neuroimaging in these processes; the review focuses on magnetoencephalography, 2-deoxy-2-[^{18}F] fluoro-D-glucose positron emission tomography, and single photon emission computed tomography. The characteristics, advantages, and disadvantages of each modality are summarized. In some cases, but not all, functional neuroimaging modalities help avoid invasive iEEG without worsening surgical outcome and aid in determining the coverage area of iEEG, thereby resulting in better outcome and less complication.

Key words : epilepsy surgery, neuroimaging, magnetoencephalography, FDG-PET, SPECT

はじめに

脳科学研究の目的は，ヒトの脳がいかに機能するかを解明し，さらに得られた知見を脳神経疾患の治療に役立てることである。高次脳機能イメージングも，脳科学研究に用いられるのみでなく，神経疾患の臨床においても欠くことのできない存在となっている。

てんかんは，患者の年齢が生下時から高齢までと幅広く，患者数の多い神経疾患である。てんかんの診断治療と脳科学との関わりには長い歴史があるが，最近の高次脳機能イメージングは，てんかんの診断治療の中でも特に外科治療の術前検査における意義が大きい。

本稿では，実際の症例を提示して，てんかん術前検査における高次脳機能イメージングの意義を検討したうえで，各検査について概説する。

Ⅰ．てんかん外科術前検査における高次脳機能イメージングの意義

現時点では，てんかん外科治療における焦点局在診断の最終基準は頭蓋内脳波である。てんかん焦点の検出力，焦点局在の空間解像度に関して，頭蓋内脳波記録に勝るものはない。これは術前の機能マッピングにおいても同様である。したがって，新しい高次脳機能イメージングの焦点局在診断における焦点検出力や焦点局在解像度は，通常，頭蓋内脳波と比較して行われる[1]。

側頭葉内側の硬化症や腫瘍・形成異常などの限局性病

* 東京大学大学院医学系研究科脳神経外科〔〒113-8655 東京都文京区本郷7-3-1〕Department of Neurosurgery, Graduate School of Medicine, the University of Tokyo, 7-3-1 Hongo, Bunkyo-ku, Tokyo 113-8655, Japan

1881-6096/12/¥500/論文/JCOPY

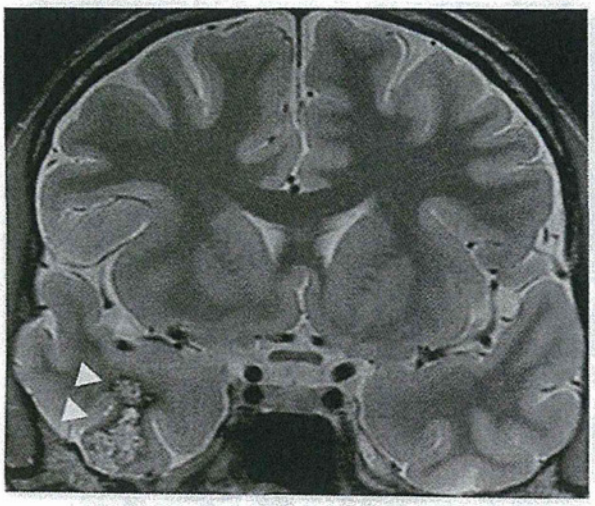

Fig. 1　症例1の術前MRI

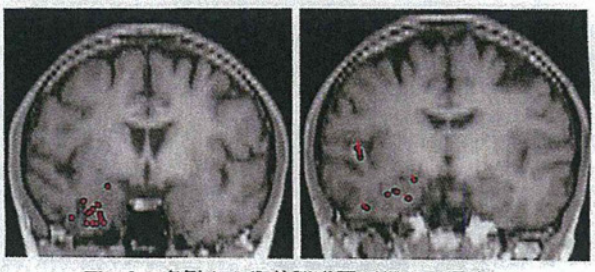

Fig. 2　症例1の術前脳磁図が捉えた電流源

変に伴う一側性側頭葉てんかんでは，MRIと脳波による診断で良好な手術成績が得られるが，MRI無病変や両側病変，脳波で両側発作起始が疑われる場合など非典型例では，両側側頭葉の頭蓋内脳波検査が必要である。新皮質てんかんや側頭葉外てんかんでは，切除範囲が広いほど発作転帰が良好であることは経験上明らかと考えられている。そのため，非優位側の前頭葉や側頭葉などでは必ずしも詳細な焦点局在診断を行わずとも広範な定型的切除で対処しうるが，機能領域とのオーバーラップが問題となるその他の領域では，頭蓋内脳波による詳細な焦点局在診断と機能局在診断が要求される。

一方，手術による頭蓋内電極の留置は侵襲的であり，合併症や患者・医療者の負担を減ずるためには，省略できる電極留置は省略し，減らせる電極は減らしたい。また，頭蓋内脳波の検出力や有用性は，どこにどれだけの電極を留置するかによって規定されるので，頭蓋内脳波検査を行う場合には，頭蓋内電極の留置範囲を適切に決めることが極めて重要である。

したがって，高次脳機能イメージングの術前検査における意義は，①その検査によって，最終的な手術転帰を変えずに，侵襲的な頭蓋内脳波検査を省略できたか，②その検査によって，頭蓋内電極の留置範囲が変わったか，③頭蓋内電極の留置範囲が変わったことにより，発作や合併症の手術転帰が改善したか，などの観点で評価される[2,3]。

以下，症例を提示しながら，てんかん術前検査における手術適応や治療手順決定の考え方を示し，そのプロセスにおける機能イメージングの意義を論ずる。

〔症例1〕MRIで限局性病変を有する側頭葉てんかん

30歳頃に複雑部分発作を発症し，抗てんかん薬多剤治療によっても抑制されないため紹介されてきた36歳女性である。発作起始の自覚はなく，突然の動作停止後，呻き声とともに唾を飲み込み，泣くような表情になる。上肢自動症があるが，側方性は明らかではない。発作は週単位で出現し，個々の発作は2～3分間持続する。頭部MRIでは右側頭葉，下側頭回の先端部に海綿状血管奇形と思われる病変が確認された（Fig. 1の△部）。長時間ビデオ脳波では，右側で蝶形骨電極＞前側頭＞中側頭の振幅で棘波が頻発するが，左側の蝶形骨電極からも低頻度の棘波が出現していた。捕捉された発作は突然の動作停止とほぼ同時に右蝶形骨電極で最大となる徐波律動を呈していた。

脳波とMRIの所見からは，右側頭葉先端部の病変に伴うてんかん原性が明白であり，右側頭葉の手術の方針でよさそうである。さらに検討するべきポイントは，病変のみの切除でよいのか，周囲脳も切除するべきか，切除するとしたらどこまで切除するか，特に海馬を含めた側頭葉内側部を切除するかどうか，などであり，そのためには，①周囲脳や内側部にどれだけてんかん原性があるか（発作起始があるか，非発作時のてんかん性活動があるか，さらにそれらと術後発作転帰との関係はどうか），②周囲脳や内側部に生理的機能があるかどうか，切除によって認知機能の低下をきたさないかどうか，を知りたい。これらの情報を得るのに最も確実な方法は頭蓋内電極を用いたてんかん性活動のモニタリングと電気刺激マッピングであるが，これをある程度代用することができないかという観点から術前検査を追加した。

頭皮脳波では，蝶形骨電極を用いても側頭葉底部からのてんかん性発射と海馬からのてんかん性発射を区別することはできない。そこで脳磁図検査を施行してみると，てんかん性棘波の電流源は病変周囲，特に紡錘状回に最も集積していた。ただし，海馬にもかなりの電流源が認められる（Fig. 2）。FDG-PETでは，病変の周囲や

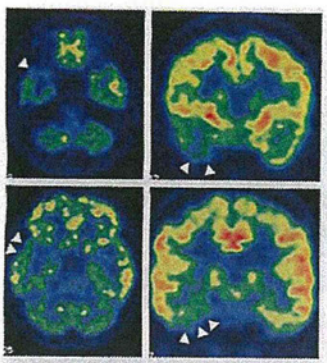

Fig. 3　症例1の術前 FDG-PET

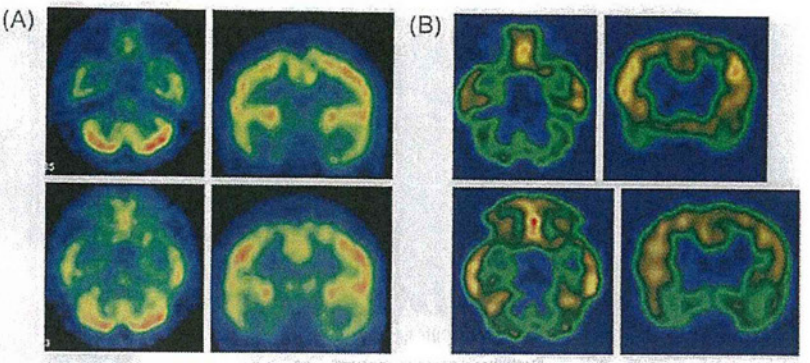

Fig. 4　症例1の術前 SPECT
A：ECD-SPECT による局所脳血流，B：イオマゼニル SPECT による中枢性ベンゾジアゼピン結合の低下領域。

側頭葉内側部でも局所糖代謝の低下が認められた（Fig. 3）。一方，ECD-SPECT による局所脳血流や，イオマゼニル SPECT による中枢性ベンゾジアゼピン結合の低下領域は，糖代謝低下領域と比較すると，より側頭葉の前底部や内側に限局しているようにみえた（Fig. 4）。なお，和田試験では言語・記憶とも左側が優位側であり，ウェクスラー記憶評価尺度は，言語性記憶 67，視覚性記憶 113，一般的記憶 77，注意/集中力 92，遅延再生 82 であった。

この患者の機能画像所見は，MRI で診断された右側頭葉の病変に伴って，脳波で診断された右側頭葉のてんかん原性を強く支持するものであり，補足的に有用である。各々の検査所見が，頭蓋内電極を省略できる強い根拠となっているわけではないが，脳波や MRI の所見，およびすべての機能画像の所見が一致しており，頭蓋内電極検査を省略した。ただし，その判断の背景には，非優位側であり詳細な言語マッピングが不要であること，頭蓋内電極で海馬からの発作起始が確認されれば海馬切除の根拠となるが，海馬からの発作起始が確認されなかった場合は海馬切除の適否の根拠とはならないこと，も存在する。

手術中には，まず，側頭葉の先端部・底面・外側面からまんべんなく皮質脳波を記録した。側頭葉先端部全体から同期する棘波が比較的頻繁にみられたほか，先端から約 3 cm の底面から高振幅棘波が極めて頻繁に出現していた。側頭葉先端部を約 3 cm まで血管腫を含めて切除し，開放された側脳室下角の先端部から海馬脳室面の脳波も記録した。病変や側頭葉先端部の切除後にもかかわらず，海馬脳室面の外側や海馬傍回から高頻度の棘波発射が認められ，海馬頭部内側や扁桃体からも比較的頻繁に棘波が出現していた。そこで，鉤部と海馬前部を追加切除した（Fig. 5）。術直後から発作は消失し，1 年半後の最終追跡時点まで無発作で経過している。術後の記憶評価尺度は，言語性記憶 86，視覚性記憶 106，一般的記憶 91，注意/集中力 107，遅延再生 90，と視覚性記憶を除く顕著な改善がみられた。視覚性記憶の軽度の低下は右海馬切除に起因すると考えられた。

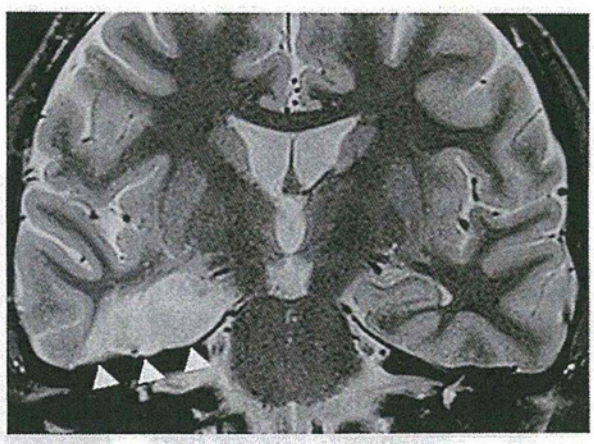

Fig. 5　症例1の手術部位
手術中の皮質脳波記録から鉤部と海馬前部を追加切除した（△部）。

（症例2）両側頭頂後頭葉の多小脳回に伴う症候性局在関連てんかん

9 歳時に意識減損発作で発症し，多種の抗てんかん薬に抵抗して日単位から週単位の複雑部分発作が続く 14 歳女児である。発作は突然の動作停止，一点凝視するもので，右側へ回転しながら右上下肢を硬直させる。発作中には口部自動症を呈する。頭部 MRI では両側頭頂葉後頭葉内側に多小脳回を認めたが側頭葉には異常はみられなかった（Fig. 6）。長時間ビデオ脳波では，非発作時には主に左の前側頭，中側頭から棘徐波が出現してお

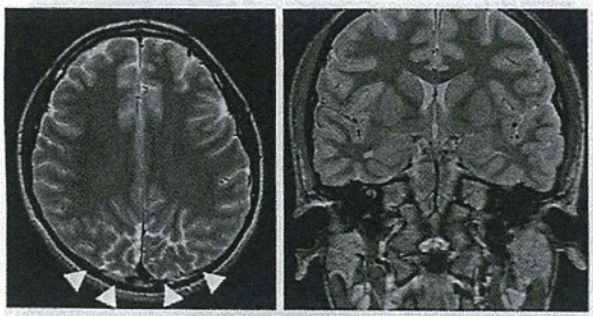

Fig. 6　症例 2 の術前 MRI

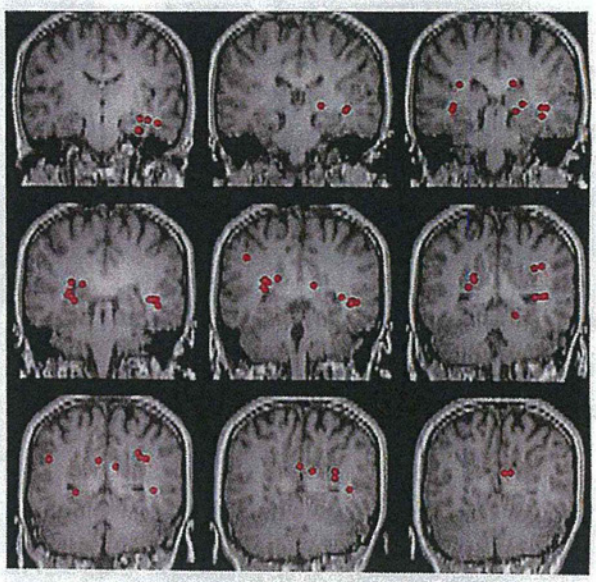

Fig. 7　症例 2 の術前脳磁図が捉えた電流源

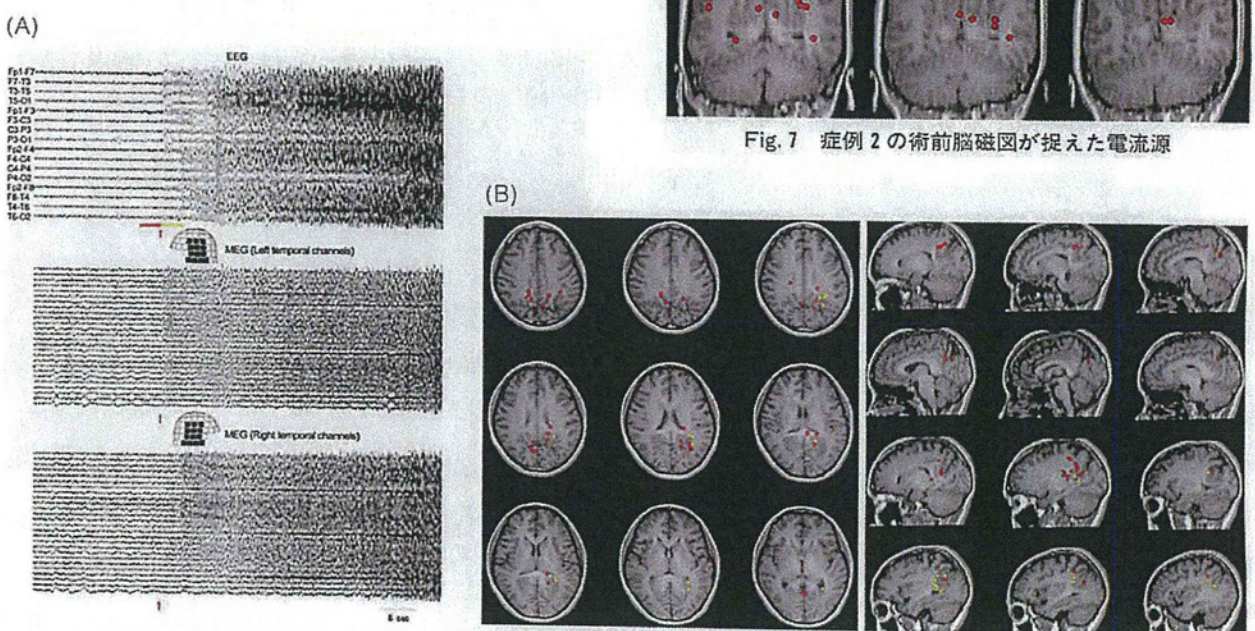

Fig. 8　症例 2 の発作時の脳波と脳磁図

脳磁図では偶然発作が捉えられた。発作起始直前と直後（各々A の黄色と赤色の横線）について電流源推定を行った（B)。発作起始直前には両側多小脳回病変で広汎に（赤点），直後には左多小脳回病変に高密度の集積が認められた（黄点)。

り，右側からの発射は稀であった。発作時には，最初の動作停止で全般性の律動性徐波がみられ，次いで左蝶形骨電極＞前側頭に律動波が観察された。視覚性の前兆はなかった。

発作症候や脳波からは左側頭葉焦点が疑われるが，MRI 病変は両側頭頂後頭葉に存在し，右利きであることから，詳細な焦点局在診断が必要と考えた。そのためには頭蓋内電極の留置が必要だが，そもそも留置の適応があるのか，さらに留置するとしたらどの範囲に留置すべきか，これまでのデータからのみでは判断し難い。

脳磁図検査を行ったところ，脳波と同様に左側頭葉前部からの棘波を認めたものの，それ以外にも両側側頭葉後部から頭頂後頭葉にかけて広汎な領域に電流源が推定された（Fig. 7)。さらに偶然，検査中に発作があり，発作時の脳磁図を記録することができた。発作時の脳波・脳磁図同時記録より発作起始前後の数秒間に対して電流源推定を行ったところ（Fig. 8 A)，発作起始直前には両側多小脳回病変に，直後には左多小脳回病変に高密度の集積がみられた（Fig. 8 B)。

FDG-PET では，左右側頭葉前方域に代謝低下を認めた。臨床発作はなかったにもかかわらず，左右頭頂後頭内側域は MRI の多小脳回に一致して集積増加が認められた（Fig. 9)。イオマゼニル SPECT では多小脳回に一致して軽度の集積増加があり，ECD-SPECT では非発作時には左半球性広汎に軽度の血流低下を認め，発作時には左半球性に血流増加を認めた。